

DISCLAIMER

This document was prepared as an account of work sponsored by the United States Government. While this document is believed to contain correct information, neither the United States Government nor any agency thereof, nor the Regents of the University of California, nor any of their employees, makes any warranty, express or implied, or assumes any legal responsibility for the accuracy, completeness, or usefulness of any information, apparatus, product, or process disclosed, or represents that its use would not infringe privately owned rights. Reference herein to any specific commercial product, process, or service by its trade name, trademark, manufacturer, or otherwise, does not necessarily constitute or imply its endorsement, recommendation, or favoring by the United States Government or any agency thereof, or the Regents of the University of California. The views and opinions of authors expressed herein do not necessarily state or reflect those of the United States Government or any agency thereof or the Regents of the University of California.

LBL-36004
UC-413

The Nuclear Thomas-Fermi Model

W.D. Myers and W.J. Świątecki

Nuclear Science Division
Lawrence Berkeley Laboratory
University of California
Berkeley, California 94720

August 1994

This work was supported in part by the Director, Office of Energy Research, Office of High Energy and Nuclear Physics, Division of Nuclear Physics, and by the Office of Basic Energy Sciences, Division of Nuclear Sciences, of the U.S. Department of Energy under Contract No. DE-AC03-76SF00098.

W.D. Myers and W.J. ŚWIĄTECKI

Nuclear Science Division

Lawrence Berkeley Laboratory

1 Cyclotron Road, Berkeley, California 94720

* Talk presented by W.J. Świątecki at the XXIX Zakopane School of Physics, 5-14 September 1994,
Zakopane, Poland.

Abstract

The statistical Thomas-Fermi model is applied to a comprehensive survey of macroscopic nuclear properties. The model uses a Seyler-Blanchard effective nucleon-nucleon interaction, generalized by the addition of one momentum-dependent and one density-dependent term. The adjustable parameters of the interaction were fitted to shell-corrected masses of 1654 nuclei, to the diffuseness of the nuclear surface and to the measured depths of the optical model potential. With these parameters nuclear sizes are well reproduced, and only relatively minor deviations between measured and calculated fission barriers of 36 nuclei are found. The model determines the principal bulk and surface properties of nuclear matter and provides estimates for the more subtle, Droplet Model, properties. The predicted energy vs. density relation for neutron matter is in striking correspondence with the 1981 theoretical estimate of Friedman and Pandharipande [1]. Other extreme situations to which the model is applied are a study of Sn isotopes from ^{82}Sn to ^{170}Sn , and the rupture into a bubble configuration of a nucleus (constrained to spherical symmetry) which takes place when Z^2/A exceeds about 100.

1. Introduction

In trying to understand astrophysical systems such as a collapsing and rebounding supernova or the resulting neutron star, one needs information concerning the properties of nuclear matter in the bulk, for example its compressibility for various values of the neutron-to-proton ratio, N/Z [2]. It would be nice to have available in the laboratory big globs of nuclear matter and to study directly these and other properties, such as the surface energy (including the curvature correction), the dependence of the surface energy on the N/Z ratio, and the binding energy curve of unbound neutron matter, for example. Since globs of nuclear matter are not available, one has to proceed indirectly, by developing a theoretical model that is fitted to finite nuclei and then extrapolating to infinite or semi-infinite nuclear matter. By asking

appropriate questions of the model one can then estimate, more or less reliably, various properties of the macroscopic nuclear fluid. What model to use? The Hartree-Fock model, quite successful for finite nuclei, is not what you really need. You cannot carry out a microscopic Hartree-Fock calculation for 10^{57} nucleons in a neutron star anyway, and even if you could, the microscopic shell effects that the calculation would produce would be that much wasted effort. What one needs is a theory like a self-consistent Hartree-Fock theory, but *without* shell effects.

The Thomas-Fermi model is just that. It is a self-consistent theory like Hartree-Fock, but averaged over shells. It was introduced into atomic physics by L.H. Thomas as early as November 1926 (published in January, 1927, [3]) and, independently, by E. Fermi a year later [4]. It is a beautiful statistical theory based on one simple fact: the Pauli exclusion principle forces a degenerate gas of fermions to populate phase space with two particles per volume h^3 of this space. Thus, for any given potential well $U(\vec{r})$, the atomic or nuclear particle density can be written down at once as proportional to the 3/2 power of the potential depth measured with respect to the Fermi level, i.e., with respect to the energy of the fastest particle. (The local phase space is proportional to the cube of the Fermi momentum P and the Fermi energy is proportional to the square of P , hence the 3/2 power.) If the resulting density is then used to generate the potential $U(\vec{r})$ by way of an appropriate law of interaction (Coulomb in the atomic case, an effective short-range force in the nuclear case), and if the potential and density are subsequently iterated to self-consistency, as in a Hartree-Fock scheme, one obtains the Thomas-Fermi approximation to the density distribution, binding energy and any other property of the system. As the title of Fermi's paper proclaims in broken English: "Un metodo statistico per la determinazione di alcune proprietà dell' atomo."

Figure 1 shows, as an example, a comparison of the Thomas-Fermi and the Hartree electronic densities for the Hg atom [5], and Fermi's calculation of the number of atomic p-electrons as a function of the atomic number Z [4]. As you can see, the Thomas-Fermi

approximation provides a wonderful pocket theory of atomic (and molecular) properties, averaged over shell effects [5].

This statistical approximation has also been applied to nuclei. As in the atomic case various improvements have been explored subsequently, bringing in density-gradient corrections and other refinements [6] and [7-13]. The most systematic such improvements are based on a formal expansion in powers of \hbar [14].

Our own work takes as its starting point the 1961 and 1963 straightforward Thomas-Fermi model of Seyler and Blanchard [15]. We too have tried various refinements of the basic Thomas-Fermi method [16, 17], but have finally decided to exploit fully the simple beauty of the original theory when aiming at a comprehensive description of a vast amount of data [18, 19]. (A comprehensive discussion of fission barriers becomes very difficult if one attempts to go beyond the basic Thomas-Fermi theory.) We have, however, improved the Seyler-Blanchard four-parameter nucleon-nucleon force [20, 21]. With two additional adjustable parameters in the force we can now give an excellent account of (shell-corrected) ground-state masses of some 1600 nuclei, as well as provide a fair description of nuclear density distributions and fission barriers. With a seventh parameter added we can also remove a serious blemish of the Seyler-Blanchard model by giving an acceptable account of the depth of the nuclear optical model potential, including its energy and isospin dependences. Having finally, after several years, frozen the adjustable parameters of the model, we are now going on with the working out of its consequences in every conceivable situation, especially for nuclei subjected to various extreme conditions. In the present talk I will describe our model and some of the currently available results.

2. The model

The total energy of a nucleus is written as an integral over all space of an energy density $\mathcal{E}(\bar{r})$, and consists of a standard Thomas-Fermi kinetic energy and an interaction energy, Coulomb plus nuclear [20]. (In the Coulomb energy we have now included the exchange

correction). The nuclear energy is a sum of neutron-neutron, proton-proton (i.e., "like") and neutron-proton (i.e., "unlike") interaction energies:

$$W_{nn \text{ or } pp} = \frac{1}{2} \int d^3r_1 \int d^3r_2 \int_{n \text{ or } p} d^3p_1 \int_{n \text{ or } p} d^3p_2 (2/h^3)^2 v_{12}(\text{like}) \quad (1)$$

$$W_{np} = \int d^3r_1 \int d^3r_2 \int_n d^3p_1 \int_p d^3p_2 (2/h^3)^2 v_{12}(\text{unlike}) \quad (2)$$

Here $2/h^3$ is the neutron or proton density in the phase spaces \bar{r}_1, \bar{p}_1 and \bar{r}_2, \bar{p}_2 for particles 1 and 2, the integrals are over those phase spaces, and $v_{12}(\text{like})$, $v_{12}(\text{unlike})$ are the effective interaction potentials between the two like or unlike particles. A clever choice of these effective interactions is a challenge to nuclear Thomas-Fermi practitioners, where art and science come together.

3. The effective interaction

We have generalized the Seyler-Blanchard interaction by adding one momentum-dependent and one density-dependent [22] term:

$$v_{12} = 2T_0\rho_0^{-1} \cdot Y(r_{12}) \cdot \left[-\alpha + \beta(p_{12}/P_0)^2 - \gamma(p_{12}/P_0)^{-1} + \sigma(2\bar{\rho}/\rho_0)^{2/3} \right] \quad (3)$$

\leftarrow
 Seyler-Blanchard
 \rightarrow

}
 }
 }

}
 }

Extra attraction increases when p_{12} is small (and particles would like to become correlated), and tends to zero for large p_{12} , when particles would zip past each other.

Repulsion increases with increasing average density $\bar{\rho}$.

In the above, the quantities T_0 , P_0 , ρ_0 are the Fermi energy, the Fermi momentum and the particle density of standard nuclear matter. (They serve as convenient units.) $Y(r_{12})$ is a normalized Yukawa interaction of range a :

$$Y(r_{12}) = \frac{1}{4\pi a^3} \frac{e^{-r_{12}/a}}{r_{12}/a} \quad (4)$$

The distance between the interacting particles is r_{12} and the magnitude of their relative momentum is p_{12} . The average density $\bar{\rho}$ is defined by

$$\bar{\rho}^{2/3} = (\rho_1^{2/3} + \rho_2^{2/3})/2, \quad (5)$$

where ρ_1 and ρ_2 are the relevant densities of the interacting particles (neutrons or protons) at points 1 and 2. The dimensionless interaction strength parameters α , β , γ , σ may be different for interactions between like and unlike particles, and the difference is described in our model by two parameters ξ and ζ , as follows:

$$\begin{aligned} \alpha_\ell &= \frac{1}{2}(1-\xi)\alpha, & \alpha_u &= \frac{1}{2}(1+\xi)\alpha, \\ \left. \begin{array}{l} \beta_\ell \\ \gamma_\ell \\ \sigma_\ell \end{array} \right\} &= \frac{1}{2}(1-\zeta) \left\{ \begin{array}{l} \beta \\ \gamma \\ \sigma \end{array} \right\}, & \left. \begin{array}{l} \beta_u \\ \gamma_u \\ \sigma_u \end{array} \right\} &= \frac{1}{2}(1+\zeta) \left\{ \begin{array}{l} \beta \\ \gamma \\ \sigma \end{array} \right\}. \end{aligned} \quad (6)$$

Altogether there are thus seven adjustable parameters in the effective interaction: α , β , γ , σ , ξ , ζ and the range a . It turns out that binding energies and density distributions depend only on six parameters because, for these properties, β and σ always occur together in the combination $B \equiv \beta + (5/6)\sigma$.

4. The optimum parameters

The parameter set that we have adopted (on the basis of the fitting procedures to be described) is as follows:

$$\alpha = 1.98483, \quad \beta = 0.15790, \quad \gamma = 1.10121, \quad \sigma = 1.05, \quad (B = 1.03290), \quad \xi = 0.25771, \quad \zeta = 0.53002, \\ a = 0.59346 \text{ fm.}$$

Anticipating what follows, we list here for the sake of completeness the values of the bulk and surface properties of nuclear matter, as deduced from the above parameter set:

Radius constant of standard nuclear matter	$r_0 = 1.14$ fm
Surface width [23] (diffuseness)	$b_0 = 1.0$ fm
Width after folding-in nucleon form factor	$b = 1.11$ fm
Volume binding energy coefficient	$a_1 = 16.04$ MeV
Symmetry energy coefficient	$J = 32$ MeV
Surface energy coefficient	$a_2 = 18.5$ MeV
Curvature correction coefficient	$a_3 = 12$ MeV
Compressibility coefficient	$K = 234$ MeV
Effective surface stiffness coefficient	$Q = 34$ MeV
Density-symmetry coefficient	$L = 50$ MeV
Symmetry anharmonicity coefficient	$M = 7$ MeV

[For the definitions of the last three (Droplet Model) coefficients consult [19]. The coefficient Q plays a role similar to the surface symmetry energy coefficient κ_s .]

5. The Euler-Lagrange equations

With the interaction specified, the total energy of the Thomas-Fermi nucleus can be written down as a functional of the densities $\rho_n(\vec{r})$, $\rho_p(\vec{r})$ and a function of the six interaction parameters:

$$E[\rho_n(\vec{r}), \rho_p(\vec{r}); a, \alpha, B, \gamma, \xi, \zeta] = \int d^3r \mathcal{E}[\rho_n(\vec{r}), \rho_p(\vec{r})] \quad (7)$$

The requirement that the energy be stationary with respect to small particle-preserving variations $\delta\rho_n(\vec{r})$, $\delta\rho_p(\vec{r})$ demands that the functional derivatives of \mathcal{E} be constant:

$$\frac{\delta\mathcal{E}}{\delta\rho_n} = L_n \quad , \quad \frac{\delta\mathcal{E}}{\delta\rho_p} = L_p \quad , \quad (8)$$

where L_n, L_p are Lagrange multipliers. We found it possible to arrange these two Euler-Lagrange equations in the form of a pair of coupled cubic expressions in $\rho_n^{1/3}$ and $\rho_p^{1/3}$, which we solve by starting with guesses for the densities and iterating to convergence. The details are in [20]. The fact that the scheme converges (usually in fewer than a dozen iterations) and is very robust (the original guesses can be very poor ones) is a piece of good luck due, we would like to believe, to the intercession in heaven of Thomas and Fermi.

Before I describe the results obtained by solving the above equations, let me show you a number of consequences of our model that can be deduced algebraically, without invoking computers.

6. Standard Nuclear Matter

You may readily verify that with our (clever) choice of effective interaction the energy per particle of standard ($\rho_n = \rho_p$) nuclear matter at density ρ is given by the following simple quintic equation [20]:

$$\eta(\rho) \equiv \frac{E/A}{T_0} = \frac{3}{5}(1-\gamma)\Omega^2 - \frac{1}{2}\alpha\Omega^3 + \frac{3}{5}B\Omega^5, \quad (9)$$

where $\Omega = (\rho/\rho_0)^{1/3}$.

For the equilibrium density, i.e., for $\Omega = 1$, the binding per particle (in units of T_0) is

$$\eta_0 = \frac{3}{5}(1-\gamma) - \frac{1}{2}\alpha + \frac{3}{5}B \quad (= -a_1/T_0). \quad (10)$$

The equilibrium condition, $d\eta/d\Omega = 0$ at $\Omega = 1$, gives

$$0 = \frac{6}{5}(1-\gamma) - \frac{3}{2}\alpha + 3B. \quad (11)$$

The compressibility coefficient K , in units of T_0 , is given by

$$\kappa \equiv K/T_0 = \left. \frac{d^2\eta}{d\Omega^2} \right|_{\Omega=1} = \frac{6}{5}(1-\gamma) - 3\alpha + 12B. \quad (12)$$

From these equations it follows that

$$\kappa = \frac{9}{5} - 15\eta_0 - \frac{9}{5}\gamma , \quad (13)$$

or

$$K = 307.31 - 66.63 \gamma \text{ MeV} , \quad (14)$$

with our choice of parameters. Thus the compressibility is a simple linear function of the parameter γ , assuming that the values of a_1 and T_0 are kept fixed. (In fact a_1 and T_0 are not subject to significant uncertainty). Figure 2 displays $\eta(\Omega)$ for a range of assumed values of K .

7. Neutron matter

A similar equation holds for the energy per neutron of neutron matter at density ρ_n

$$\eta(\rho_n) = \frac{3}{5}(1-\gamma_\ell)\Phi^2 - \frac{1}{2}\alpha_\ell\Phi^3 + \frac{3}{5}B_\ell\Phi^5 , \quad (15)$$

where $\Phi = (\rho_n / \frac{1}{2}\rho_0)^{1/3}$ gives the density ρ_n relative to its value for standard nuclear matter. Figure 3 displays $\eta(\Phi)$ for various choices of the ratio of like to unlike interaction strengths.

8. General nuclear matter ($\rho_n > \rho_p$)

Consider nuclear matter with a fixed ratio of N/Z , i.e., a fixed relative neutron excess $I = (N-Z)/A = (\rho_n - \rho_z)/\rho$. It turns out that the energy per particle as a function of the density can still be written in the form

$$\eta(\rho) = \frac{3}{5}(1-\bar{\gamma})\Omega^2 - \frac{1}{2}\bar{\alpha}\Omega^3 + \frac{3}{5}\bar{B}\Omega^5 , \quad (16)$$

where, as before, $\Omega = (\rho/\rho_0)^{1/3}$, but where the coefficients $\bar{\gamma}$, $\bar{\alpha}$, \bar{B} are now given in terms of I by the following expressions:

$$1-\bar{\gamma} = \frac{1}{2}(1-\gamma_\ell)(p^5 + q^5) - \frac{1}{4}\gamma_u p^2 q^3 (5p^2 q^3 - q^5) \quad (17)$$

$$\bar{\alpha} = \frac{1}{2}\alpha_\ell(p^6 + q^6) + \alpha_u p^3 q^3 \quad (18)$$

$$\bar{B} = \frac{1}{2}B_\ell(p^8 + q^8) + \frac{1}{2}B_u p^3 q^3 (p^2 + q^2) , \quad (19)$$

where $p^3 = 1 + I$ and $q^3 = 1 - I$. (See Fig. 4.) Thus the dependence of the energy on density is in all cases the same type of quintic and the equilibrium condition always reduced to a readily solvable cubic. It follows that the equilibrium density, binding, as well as the compressibility coefficient $K(I)$ can be written down algebraically for any value of the relative neutron excess I .

9. Finite nuclei

Figure 5 shows the charge densities for ^{56}Fe , ^{124}Sn and ^{209}Bi , as obtained by numerically solving the Euler-Lagrange equations (8). The densities shown were obtained by folding into the calculated point densities a Yukawa proton form factor with an RMS size of 0.85 fm. The resulting values of $\langle r^2 \rangle^{1/2}$ for the three charge distributions are 3.69, 4.64, 5.51 fm, to be compared with 3.80, 4.69, 5.51 fm, or 3.73, 4.67, 5.52 fm, as deduced from [24] using a Woods-Saxon or a three-parameter Gaussian fit to electron scattering data, respectively.

10. Semi-infinite nuclear matter

By solving the Euler-Lagrange equations in the limit of semi-infinite geometry ([19], [20]) one can study the surface properties of nuclear matter. Figure 6 (based on the 1990 version of our model [20]) shows a remarkable feature of such calculations: if the surface width (diffuseness) is held fixed, the surface energy is virtually a perfectly linear function of the compressibility K . Our current model with $b_0 = 1.0$ fm gives for the width b (after folding in the nucleon size) the value $b = \sqrt{b_0^2 + (0.85)^2} / 3 = 1.11$ fm. Thus the current surface energy $a_2 = 18.5$ MeV and compressibility $K = 234$ MeV are in line with the 1990 systematics of Fig. 6.

11. Fitting ground state masses

We write the mass excess of a nucleus as [25]

$$\begin{aligned} \text{Mass excess} = & T.F. + M_n N + M_H Z + \text{Shell Correction} \\ & + \text{Even - odd Term} + \text{Wigner Term} - 0.00001433 Z^{2.39} \text{ MeV} \end{aligned} \quad (20)$$

Here T.F. is the calculated binding energy in the Thomas-Fermi model and M_n , M_H are the masses of the neutron and of the Hydrogen atom. The "Shell Correction" is taken from [26] (column headed E_{mic}).

For the even-odd term we took $\pm 11/\sqrt{A}$ MeV for odd or even nuclei and zero for odd-mass nuclei, as in [25]. We also reverted to the 1965 form of the Wigner term: $-7 \text{ MeV exp}(-6|N-Z|/A)$. The last term in Eq. 20 allows for the binding energy of the atomic electrons. Using the measured mass excesses of 1654 nuclei, we used Eq. 20 to convert them into experimental macroscopic binding energies (i.e., energies corrected for shell effects, the even-odd term, the Wigner term and electronic bindings) which then served as a "target" for the macroscopic Thomas-Fermi theory. The RMS deviation of the calculated and target binding energies was then minimized with respect to five variables. (Five and not six because one combination of the six adjustable parameters was always constrained in such a way that the surface width b_0 of standard semi-infinite nuclear matter would have the value 1.0 fm.)

I skip the technical details of these fits, which you can imagine are pretty formidable, considering that one is trying to fit 1654 nuclear masses (each one requiring for its determination up to a dozen iterations of coupled neutron and proton densities) by searching in a space of 6 parameters, with a constraint whose formulation requires another iterative Thomas-Fermi solution of a semi-infinite distribution. However, by using some tricks and shortcuts, we succeeded. The resulting optimum parameters and associated nuclear properties are listed in Section 4. The final RMS deviation for the 1654 masses was 0.711 MeV. Figure 7 compares the residual deviations between measured and calculated masses for the shape-dependent Droplet Model [26], (RMS = 0.681 MeV), and for the present Thomas-Fermi model.

Having optimally fitted the ground state masses by varying parameters that include the radius constant r_0 , two crucial questions present themselves: Will the nuclear sizes disagree

with measurements? Will the calculated fission barriers be in disastrous disagreement with measurements, as seemed to be the case in [21]? As described in Section 8, the sizes of the proton charge distributions are just fine when the optimum radius constant $r_0 = 1.14$ is used. To calculate fission barriers is much more difficult, because one needs to solve the Thomas-Fermi equations for shapes devoid of spherical symmetry.

12. Fission barriers

We solved the Euler-Lagrange equations on a three-dimensional lattice, without parameterizing the density distributions, as illustrated in Fig. 8 taken from [21]. This is a really tough proposition because even a fast computer runs out of steam when the lattice spacing is less than about 0.5 fm. This is of the order of the range of the effective interaction, and therefore not good enough for the required precision if straightforward numerical integrations are used. It is only after we applied special tricks to get solutions accurate to a fraction of an MeV (typically out of a thousand or so) that we could calculate saddle-point shapes and fission barriers despite the coarse grid. Three such saddle shapes are shown in Fig. 9. Figure 10 illustrates the calculation of a number of fission barriers, using the parameter set of [21]. Each point represents the energy of self-consistently iterated shapes, constrained to have a pre-assigned separation between the centers of mass of their two halves. Figure 11 shows a recent comparison of calculated and measured barriers (corrected for ground state shell effects) for 36 nuclei. In the region of the very heavy elements the agreement with measurements is perfect, with a slight overestimate in the lighter region. Figure 12 shows the calculations extended down to very light systems. For these nuclei unambiguous fission barrier measurements are difficult and, before making comparisons with measurements, one ought to allow for the virtual doubling of the Wigner term [27], as well as for the emergence of fragment shell and pairing effects in the severely necked-in saddle shapes in question.

13. Optical model potential depths

Figure 13 shows a comparison of measured optical model potential depths from [28] with the Thomas-Fermi calculations. At this stage all the parameters except σ were frozen at the values deduced from fitting ground state masses and the surface diffuseness, so what you see is a one-parameter fit to the depths. This is another example where our model provides a closed formula for the property in question. According to our model the potential depth $U(\tau)$ felt by a nucleon with kinetic energy τT_0 traveling through standard nuclear matter is given by

$$U(\tau)/T_0 = -\alpha + \frac{3}{5}\beta + \frac{4}{3}\sigma + \beta\tau - \gamma \begin{cases} \tau^{-1/2} & \text{for } \tau > 1 \\ \frac{3}{2} - \frac{1}{2}\tau & \text{for } \tau < 1 \end{cases} \quad (21)$$

The total energy of the nucleon is $E = U + \tau T_0$, so Eq. 21 provides an explicit relation between U and E , which is plotted in Fig. 13. Again, the agreement with measurements is close, though not perfect.

At this stage we decided to freeze our parameter set at the values listed in Section 4 and to explore the predictions of our model under various extreme conditions. Here are three examples.

14. Nuclei at the drip lines

Figure 14 shows the neutron and proton chemical potentials for isotopes of Sn from neutron number $N = 120$ down to $N = 32$. The former is the last isotope which, in the Thomas-Fermi model without shell and pairing corrections, would be stable against neutron emission. The latter, for which the proton chemical potential is plus 8.24 MeV, would be unstable against proton radioactivity by quantal barrier penetration, but would be classically metastable. Figure 15 shows the neutron and proton density distributions for ^{82}Sn , ^{120}Sn and ^{170}Sn .

15. How unbound is neutron matter?

The energy per particle of neutron matter is given by Eq. 15, which leads to

$$E_n(\rho_n) = 16.464\Phi^2 - 13.635\Phi^3 + 5.391\Phi^5 \text{ MeV} . \quad (22)$$

Figure 16 compares this prediction with the theoretical estimate of [1]. The similarity of the two curves is quite remarkable. The physical ingredients in the two methods are quite different, and they both represent bold extrapolations from measured properties of nuclear interactions and bindings to the extreme conditions prevailing in neutron matter. (It is essential to stress that, in contrast to our paper of 1990 [20], the parameters of our present Thomas-Fermi model were *not* constrained to agree with the results of [1]. They were fitted to ground-state masses and to the surface diffuseness, and the extrapolation to neutron matter agrees then with [1] without any readjustments.)

16. A nuclear bubble

It has been known for a long time [29, 30] that a sufficiently highly charged idealized nucleus, if constrained to spherical symmetry, would eventually rupture into a bubble configuration. In the simplest liquid drop model, a bubble configuration first appears when the fissility parameter x exceeds the value 2.0216 [29]. [Implying that, very roughly, $(Z^2/A)/50$ exceeds 2.0216. Stability against fission is lost at $x = 1$, i.e., when $Z^2/A \approx 50$]. The energy of the bubble configuration falls below that of the unruptured sphere when $x > 2.212$ [29]. As an illustration of this phenomenon we carried out a series of Thomas-Fermi calculations, starting with $N = 600$, $Z = 400$, and reducing the mass number A down from 1000, while keeping $(N-Z)/A$ at the fixed value of 0.2. In this way we located approximately the point where the Thomas-Fermi solution would switch from an unruptured nucleus to a bubble configuration with increasing Z^2/A . Figure 17 shows the last solid nucleus for $N = 372$, $Z = 248$ ($Z^2/A = 99.2$) and the first bubble configuration for $N = 378$, $Z = 252$ ($Z^2/A = 100.8$).

Summary and conclusions

We applied the statistical method, introduced for atomic electrons by Thomas and by Fermi, to a comprehensive description of nuclear properties. We did this by generalizing the

Seyler-Blanchard effective nucleon-nucleon force. We fitted five of the six adjustable parameters of the force to nuclear binding energies corrected for shell and pairing effects and for the Wigner term, using the sixth parameter to keep the width of the surface diffuseness at $b_0 = 1.0$ fm. The resulting RMS error in the mass fit was 0.711 MeV, comparable to the fit obtained with the shape-dependent Droplet Model of [26]. Using the resulting parameter set, we found that the sizes of nuclear charge distributions were in agreement with measurements and that fission saddle point energies of elements down to $Z = 71$ could be reproduced with only relatively minor (though systematic) discrepancies. The extrapolated binding properties of neutron matter turned out to be in striking correspondence with the theoretical estimate of [1]. Introducing a seventh (density-dependence) parameter in the effective interaction, we were able to give a fair account of the nuclear optical model potential.

On a finer scale there are, to be sure, systematic discrepancies in the trends of fission barriers, density distribution profiles and the optical model potential. Some might be due to imperfections in the effective interaction, some are surely due to the approximate nature of the Thomas-Fermi treatment. But overall we now have available a robust statistical model that shows a good correspondence with a large and varied amount of data on finite nuclei. We believe that the resulting predictions for the bulk and surface properties of nuclear matter, listed in Section 4, should be quite reliable as regards the principal (liquid drop) parameters r_0, a_1, a_2, J , and to provide fair estimates of the remaining more subtle (Droplet Model) quantities.

We will continue studying nuclei under extreme conditions of charge, isospin and, especially, angular momentum, using, as Fermi would have said, "Un metodo statistico per la determinazione di alcune proprietà del nucleo."

Acknowledgments

We would like to thank P. Möller and J.R. Nix for help with accessing the data on nuclear masses and shell effects, and for many discussions extending over several years. Jan

Černohorsky was always ready to help with computer-related problems, for which we thank him.

This work was supported by the Director, Office of Energy Research, Office of High Energy and Nuclear Physics, Division of Nuclear Physics, and by the Office of Basic Energy Sciences, Division of Nuclear Sciences, of the U.S. Department of Energy under Contract No. DE-AC03-76SF00098.

Figure captions

Fig. 1. The upper part shows a comparison between the Thomas-Fermi and the Hartree densities (multiplied by r^2) of the electrons in a Hg atom [5]. The lower part shows Fermi's prediction of the number of p-electrons as a function the atomic number Z (solid line) and the actual numbers (dashed line) [4].

Fig. 2. The binding energy of standard nuclear matter versus the cube root of the relative density, as given by Eq. (9), for different values of the compressibility K . (From [20].)

Fig. 3. The relative energy per particle of neutron matter vs. the density parameter Φ , as given by Eq. (15), for different values of the parameter ξ . For each value of ξ the other interaction parameters were re-adjusted to keep the binding, density and symmetry energy of standard nuclear matter fixed. (From [20].)

Fig. 4. The energy per particle of nuclear matter according to Eq. (16), vs. the relative density parameter Ω , for different values of the relative neutron excess $\delta \equiv (\rho_n - \rho_p)/(\rho_n + \rho_p)$. The squares are the theoretical estimates from [1]. This figure is from the 1990 version of our model [20] in which the parameters were adjusted for approximate agreement of the $\delta = 0$ curve with [1]. The current model, in which no such constraint was imposed, is illustrated in Fig. 16.

Fig. 5. The Thomas-Fermi charge distributions for ^{56}Fe , ^{124}Sn and ^{109}Bi (solid lines) are compared with electron scattering measurements as represented by a Woods-Saxon fit (dot-dashed) or a three-parameter Gaussian fit (dashed) to the data. The current parameter set, listed in Sec. 4, was used.

Fig. 6. Each set of symbols represents the result of calculating the surface energy of semi-infinite nuclear matter using interaction parameters adjusted to give the same bulk binding and density, as well as the same surface width b , but different compressibility K . There results an astonishingly linear relation between K and the surface coefficient a_2 . (From [20].)

Fig. 7. The residual deviations between measured and calculated masses when the shape-dependent Droplet Model is used for the macroscopic part (upper part) and when the present Thomas-Fermi model is used (lower part). Lines connect isotopes of a given element.

Fig. 8. One octant of the three-dimensional lattice used to solve numerically the Euler-Lagrange equations for saddle shapes. Here the neutron density for the saddle shape of ^{229}Np is depicted by displaying at each lattice point a small sphere whose radius is proportional to the local density there. (From [21].)

Fig. 9. Illustration of the saddle-point shapes for ^{166}Yb , ^{194}Hg , and ^{229}Np calculated in [21]. The upper part is a three-dimensional rendering and the lower parts are contour plots of the neutron density ρ_n corresponding to $\rho_n/(\frac{1}{2}\rho_0) = 0.2, 0.4, 0.6, 0.8, 1.0$.

Fig. 10. Deformation energies for five nuclei calculated in [21]. The constraint parameter Δ is half the distance between the centers of mass of the two halves of the nuclear shape, less its value for the spherical configuration. The current calculations are qualitatively similar, but the calculated fission barrier heights are now in much better agreement with measurements.

Fig. 11. Thirty-six calculated fission barrier heights from ^{173}Lu to ^{252}Cf (open diamonds) are compared with measurements corrected for ground-state shell effects (squares). The triangles show the difference. The "fissility" was chosen as $(Z^2/A)/(1-2.2 I^2)$, where the coefficient 2.2 multiplying the square of the relative neutron excess I was adjusted to make the calculated points conform closely to a single curve.

Fig. 12. This is like Fig. 11, but the calculations were continued all the way down to ^8Be at "fissility" = 2. The other calculated points below fissility = 30 are for ^{20}Ne , ^{40}Ca , ^{75}Br , ^{94}Mo , ^{132}Ba , and ^{160}Dy . Here, and in Fig. 11, a parameter set with $r_0 = 1.145$ rather than $r_0 = 1.14$ was used. With the canonical set based on $r_0 = 1.14$, the barrier for ^{252}Cf would be 0.19 MeV higher and for ^{173}Lu 0.41 MeV higher.

Fig. 13. The compilation of measured optical model potential depths (corrected for Coulomb effects and neutron excess, [28]) is compared with the Thomas-Fermi calculation.

Fig. 14. The proton (solid squares) and neutron (open squares) chemical potentials for the full range of Sn isotopes, from $N = 32$ to $N = 120$, for which Thomas-Fermi solutions exist.

Fig. 15. The neutron (solid line) and proton (dashed line) density distributions for ^{82}Sn , ^{120}Sn , and ^{170}Sn .

Fig. 16. Two independent predictions of the energy per particle of neutron matter. The density parameter is the cube root of the neutron density relative to its value, $\rho_0/2$, in standard nuclear matter. The squares are from [1]. The curve is the Thomas-Fermi calculation with the canonical parameter set.

Fig. 17. The upper part is the last unruptured nucleus ($N = 372$, $Z = 248$) and the lower part the first bubble nucleus ($N = 378$, $Z = 252$) in a sequence where A is increased while $(N-Z)/A$ is held fixed at the value 0.2. The parameter set from [20] was used.

References

- [1] B. Friedman and V. R. Pandharipande, *Nucl. Phys. A* **361**, 502 (1981).
- [2] M. Pi, X. Viñas, M. Barranco, A. Perez-Canyellas and A. Polls, *Astron. Astrophys. Suppl. Ser.* **64**, 439 (1986).
- [3] L. H. Thomas, *Proc. Cambridge Phil. Soc.* **33**, 542 (1927).
- [4] E. Fermi, *Rend. Lincei* **6**, 602 (1927); *Zeit. f. Physik* **48**, 73 (1928).
- [5] P. Gombas, "Die statistische Theorie des Atoms und ihre Anwendung" (Springer, Wien, 1949).
- [6] M. Brack, C. Guet and H.-B. Hakansson, *Phys. Rep.* **123**, 275 (1985).
- [7] K. A. Brueckner, J. H. Chirico and H. W. Meldner, *Phys. Rev. C* **4**, 732 (1971).
- [8] A. K. Dutta, J.-P. Arcoragi, J. M. Pearson, R. Behrman and F. Tondeur, *Nucl. Phys. A* **458**, 77 (1986).
- [9] F. Tondeur, A. K. Dutta, J. M. Pearson and R. Behrman, *Nucl. Phys. A* **470**, 93 (1987).
- [10] J. M. Pearson, Y. Aboussir, A. K. Dutta, R. C. Nayak, M. Farine and F. Tondeur, *Nucl. Phys. A* **528**, 1 (1991).
- [11] Y. Aboussir, J. M. Pearson, A. K. Dutta and F. Tondeur, *Nucl. Phys. A* **549**, 155 (1992).
- [12] F. Garcias, M. Barranco, J. Nemeth and C. Ngô, *Phys. Lett. B* **206**, 177 (1988).
- [13] F. Garcias, M. Barranco, J. Nemeth, C. Ngô and X. Viñas, *Nucl. Phys. A* **495**, 169 (1989).
- [14] P. Ring and P. Schuck, "Nuclear Many Body Problem," Springer-Verlag, New York/Berlin, 1980.
- [15] R. G. Seyler and C. H. Blanchard, *Phys. Rev.* **124**, 227 (1961); **131**, 355 (1963).
- [16] W. J. Swiatecki, *Proc. Phys. Soc. (London)* **A 68**, 285 (1955).
- [17] W. J. Swiatecki, *Nucl. Phys. A* **542**, 195 (1992).
- [18] W. D. Myers, in "Proceedings, Third Int. Conf. on Atomic Masses, Winnipeg, Canada, Aug. 28-Sept. 1, 1967" (R. C. Barber, Ed.), pp. 61-84.
- [19] W. D. Myers and W. J. Swiatecki, *Ann. Phys. (N.Y.)* **55**, 395 (1969).

- [20] W. D. Myers and W. J. Swiatecki, *Ann. Phys. (N.Y.)* **204**, 401 (1990).
- [21] W. D. Myers and W. J. Swiatecki, *Ann. Phys. (N.Y.)* **211**, 292 (1991).
- [22] D. Bandyopadhyay and S. K. Samaddar, *Nucl. Phys. A* **484**, 315 (1988).
- [23] R. W. Hasse and W. D. Myers, "Geometrical Relationships of Macroscopic Nuclear Physics," Springer-Verlag, New York/Berlin, 1988.
- [24] H. de Vries, C. W. Jager and C. de Vries, *At. Data Nucl. Data Tables* **36**, 495 (1987).
- [25] W.D. Myers and W. J. Swiatecki, *Nucl. Phys.* **81**, 1 (1966).
- [26] P. Möller, J. R. Nix, W. D. Myers and W. J. Swiatecki, "Nuclear Ground State Masses and Deformations," Los Alamos preprint LA-UR-93-3083, Aug. 16, 1993, to be published in the *Atomic Data and Nuclear Data Tables*.
- [27] W. D. Myers, "Droplet Model of Atomic Nuclei," IFI/Plenum, New York, 1977.
- [28] M. Bauer, E. Hernández-Saldaña, P. E. Hodgson and J. Quintanilla, *J. Phys. G: Nucl. Phys.* **8**, 525 (1982).
- [29] W. J. Swiatecki, Ph.D. Thesis, University of Birmingham, October 1949.
- [30] W. J. Swiatecki, *Physica Scripta* **28**, 349 (1983).

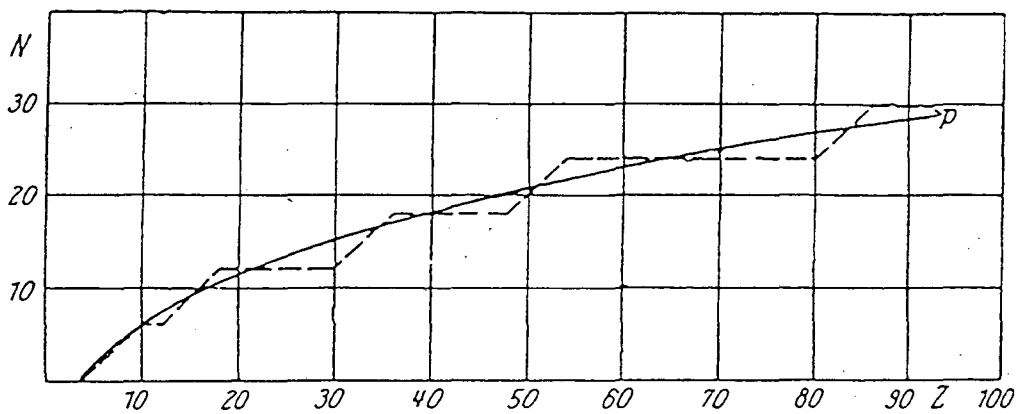
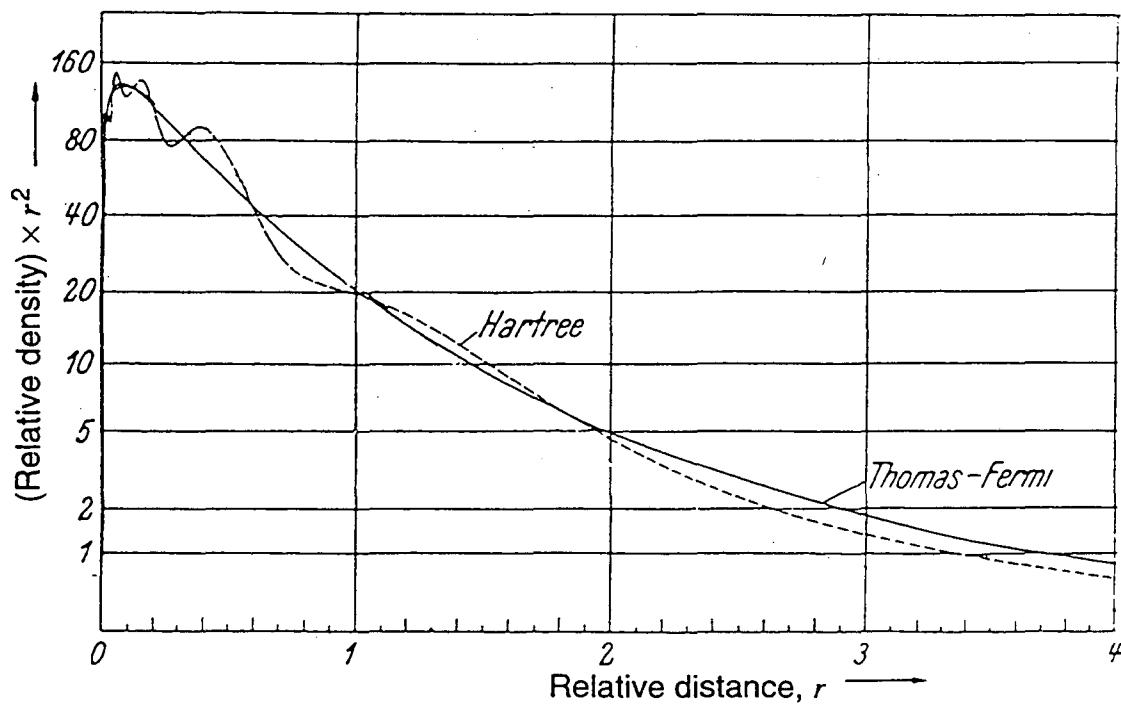


Figure 1

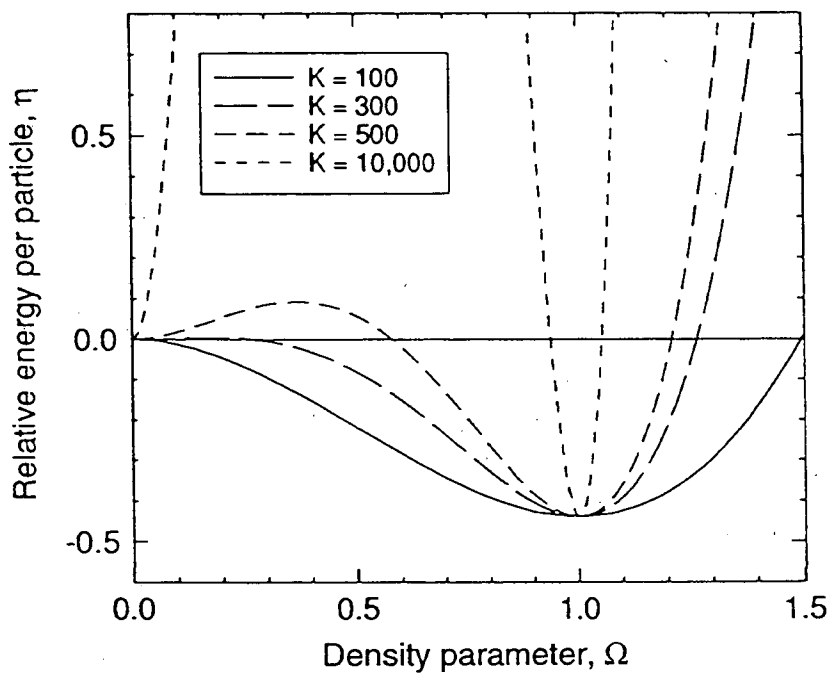


Figure 2

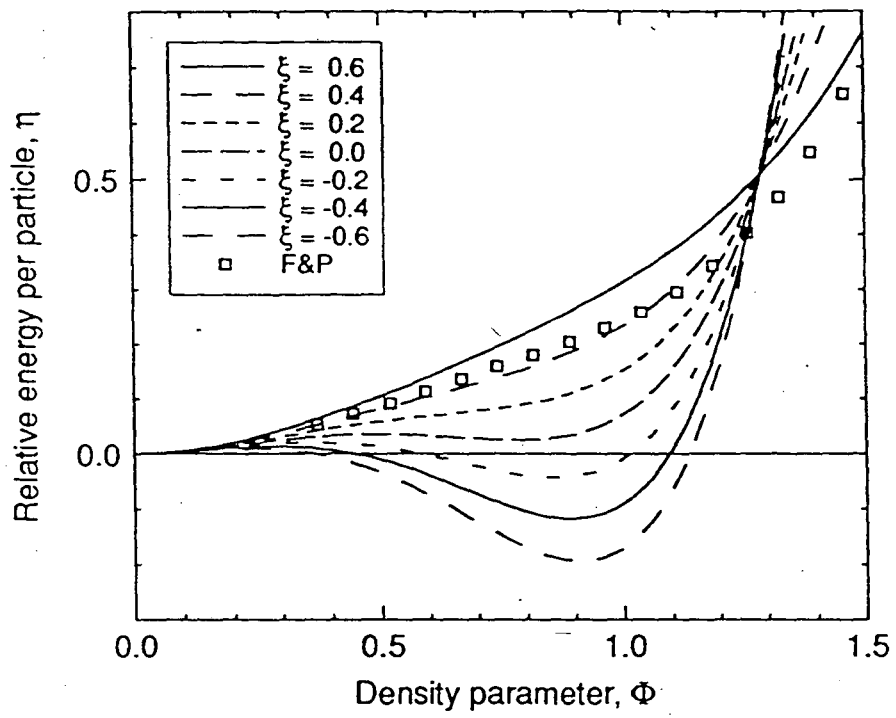


Figure 3

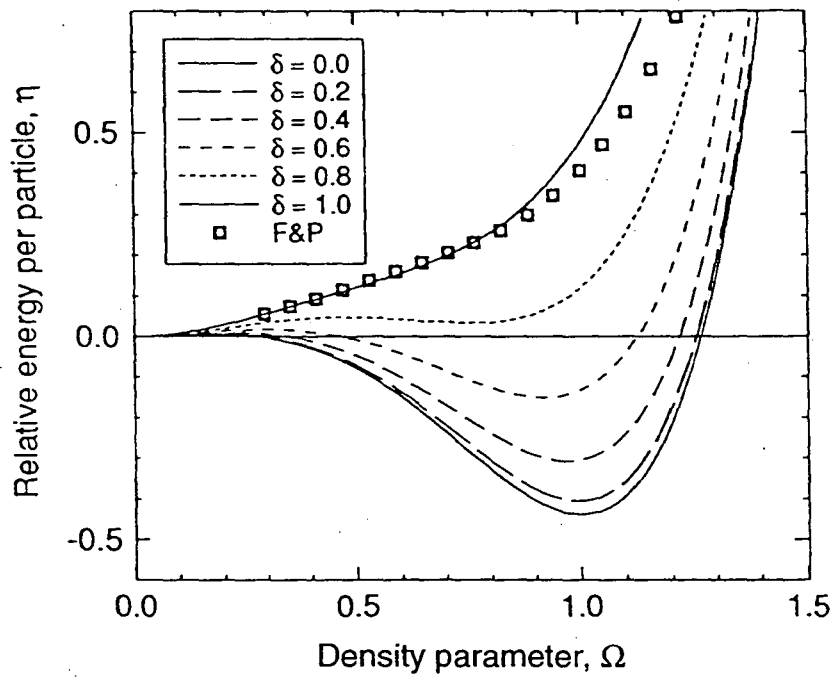


Figure 4

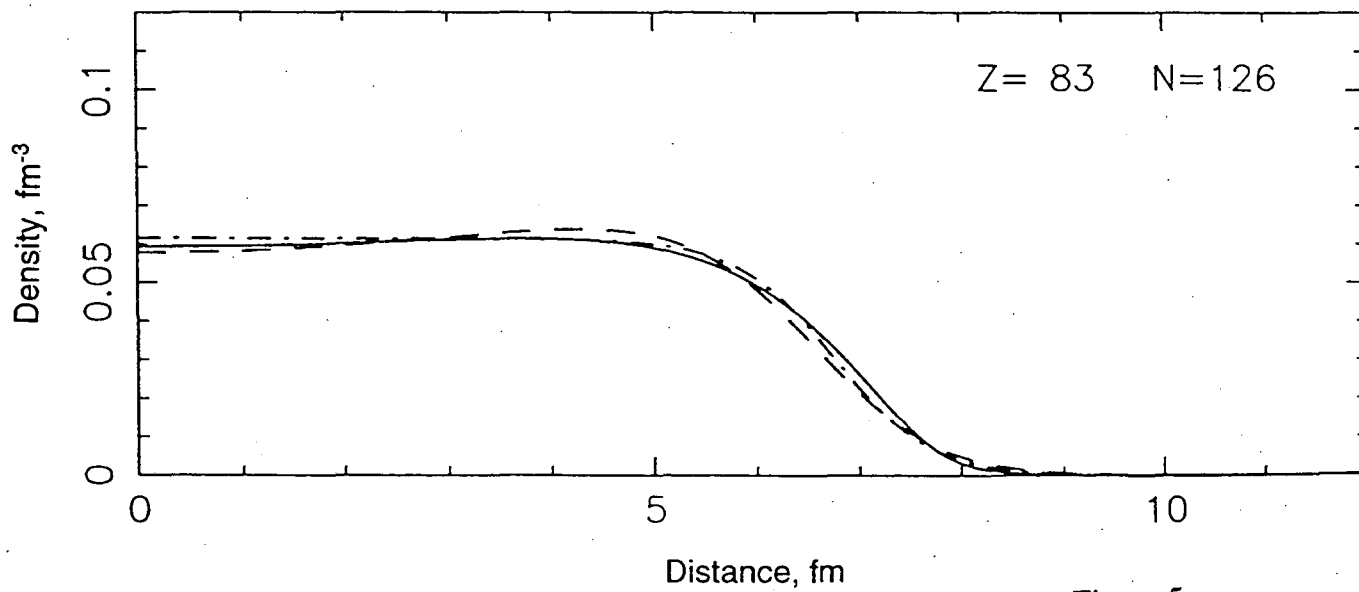
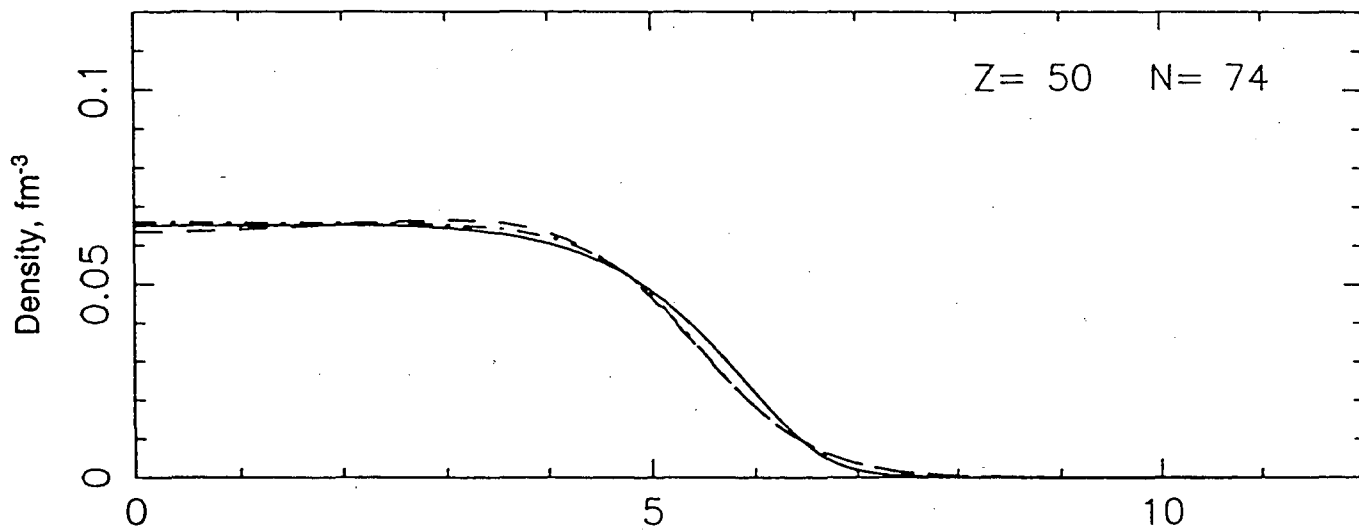
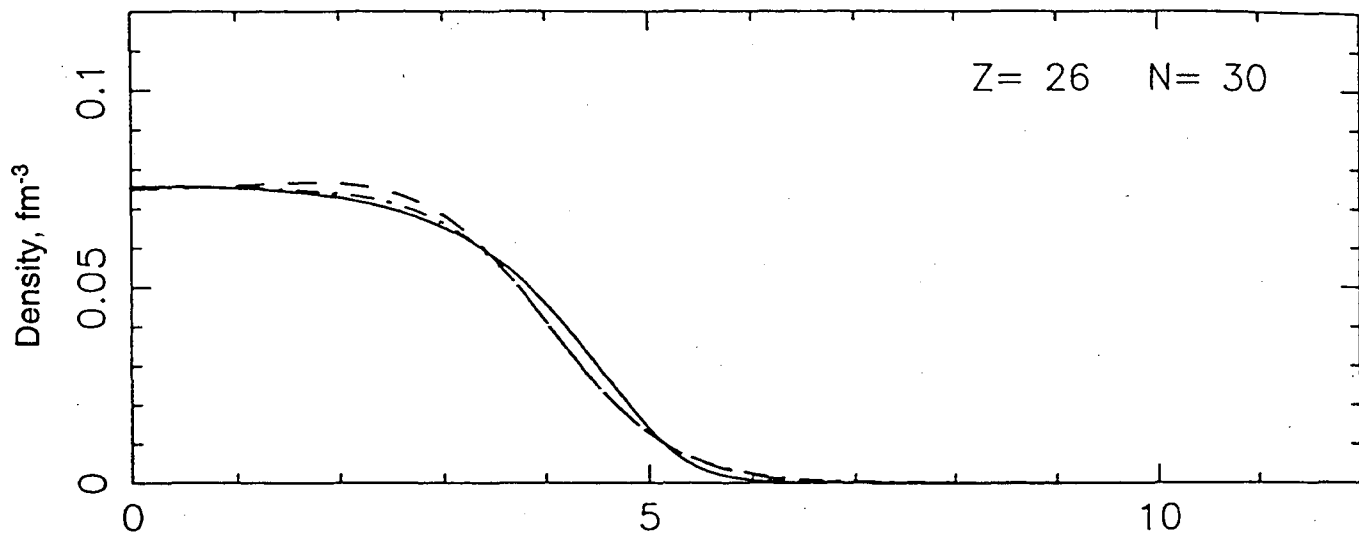


Figure 5

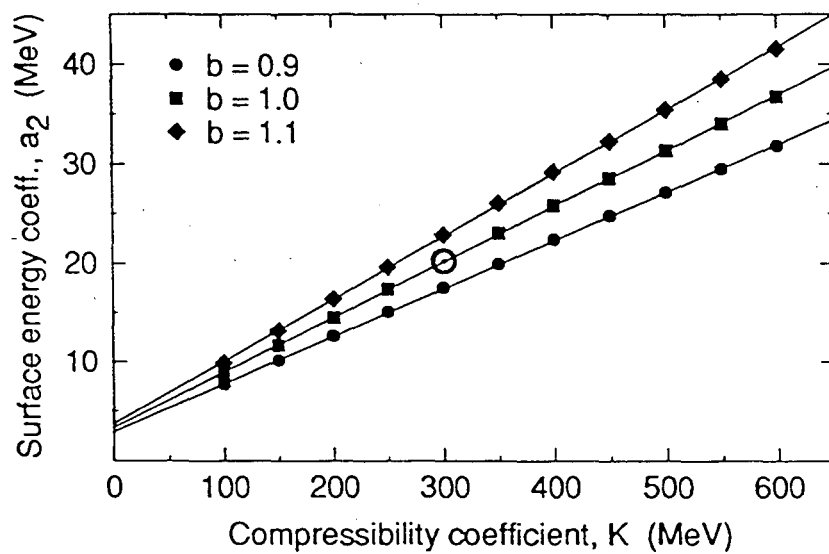


Figure 6

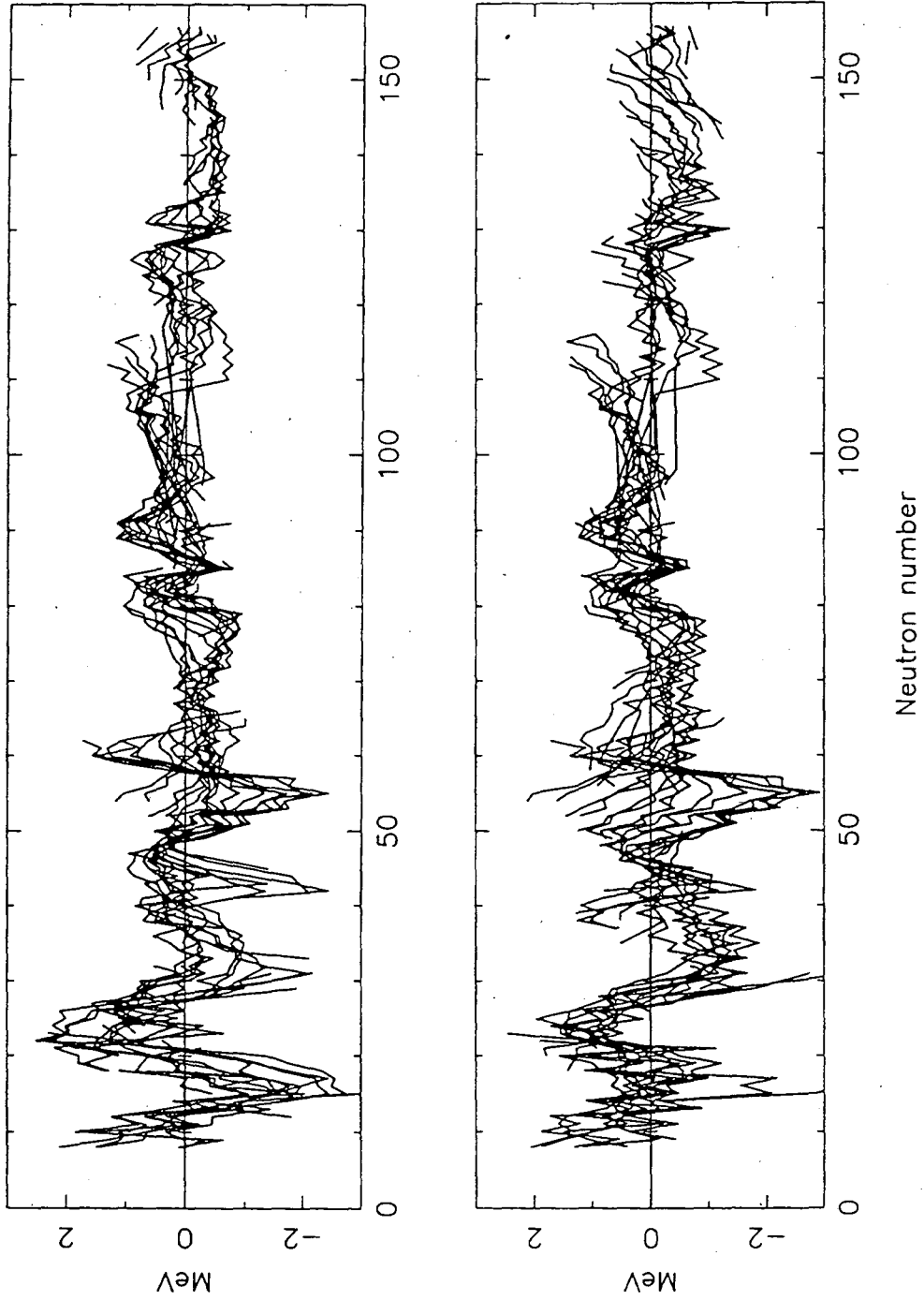


Figure 7

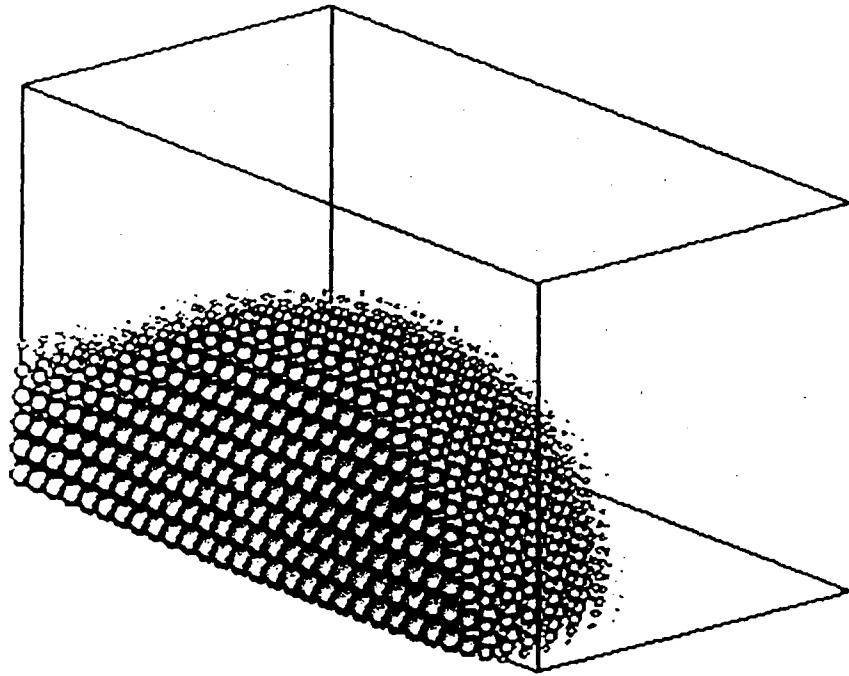
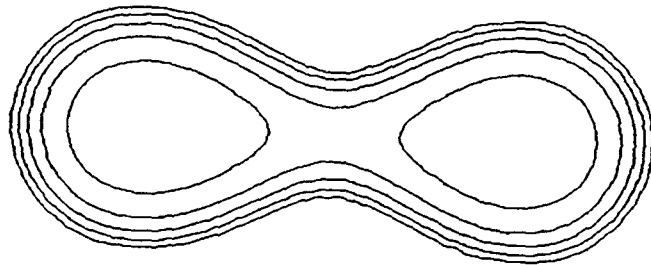


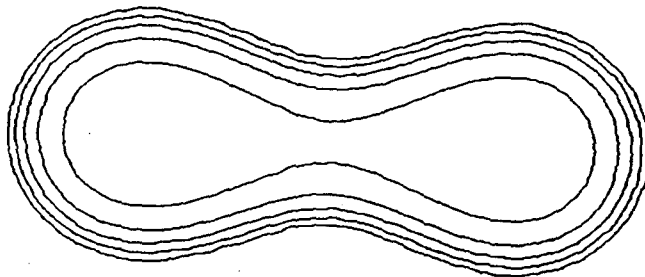
Figure 8



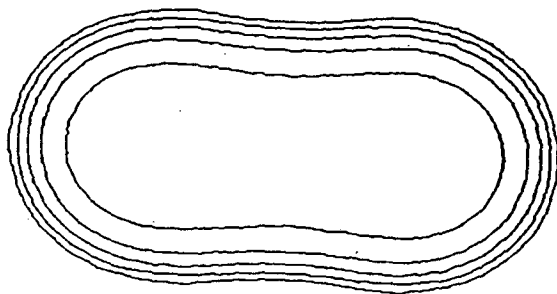
$Z = 70$
 $N = 96$



$Z = 70$
 $N = 96$



$Z = 80$
 $N = 114$



$Z = 93$
 $N = 136$

Figure 9

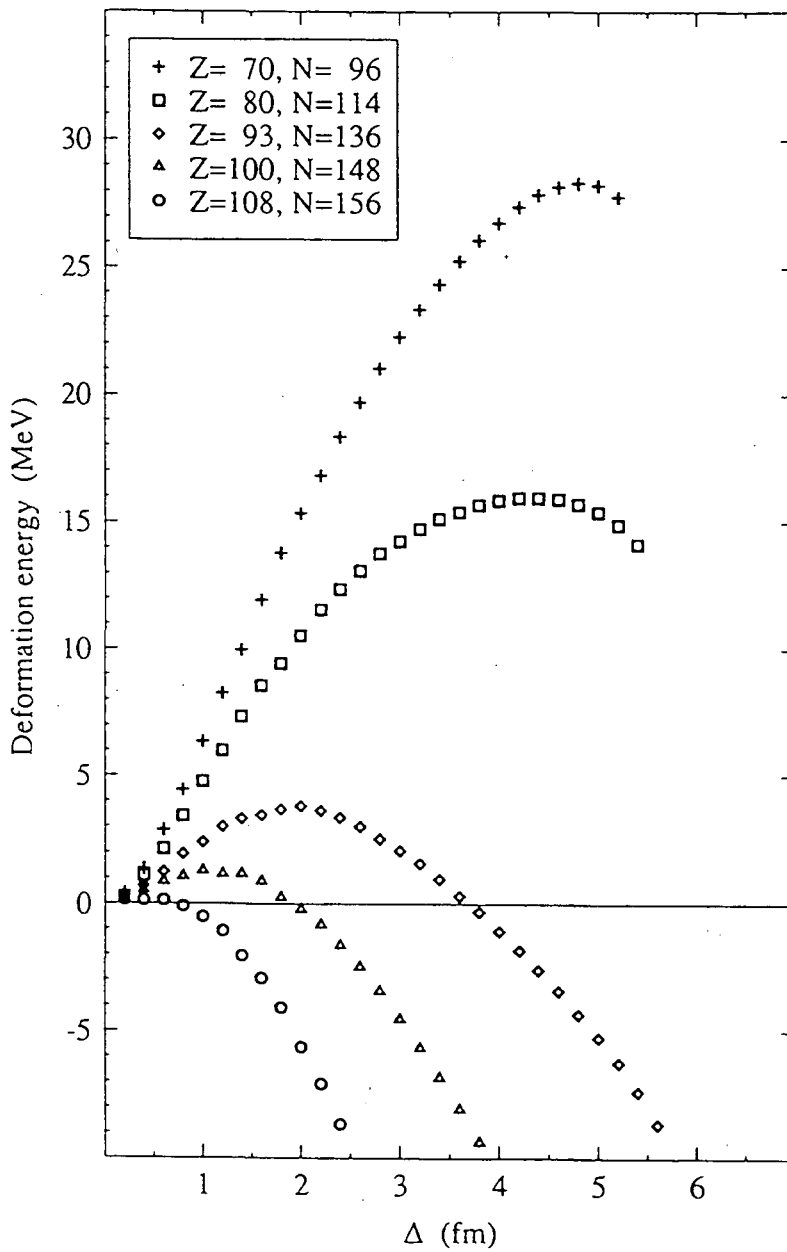
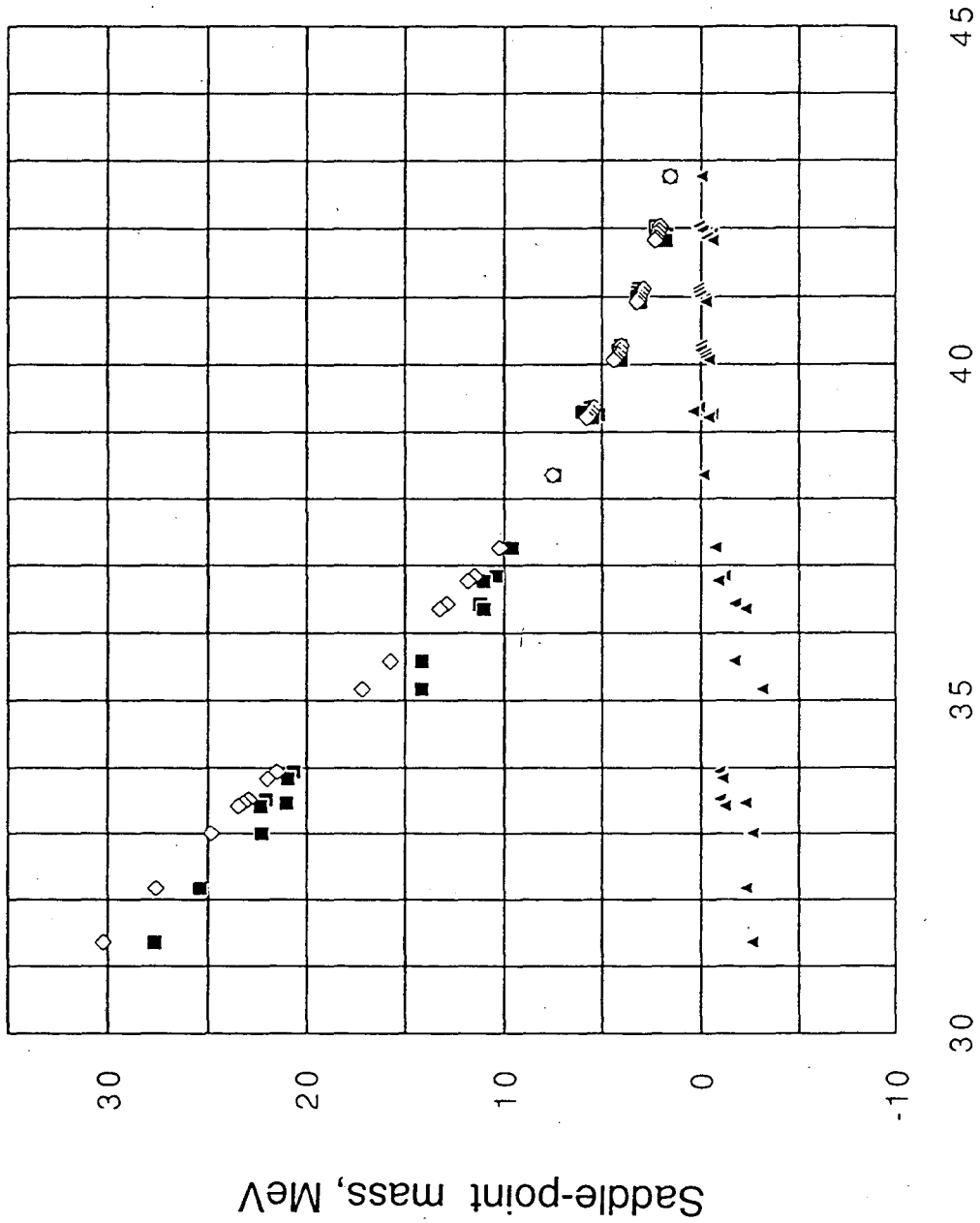
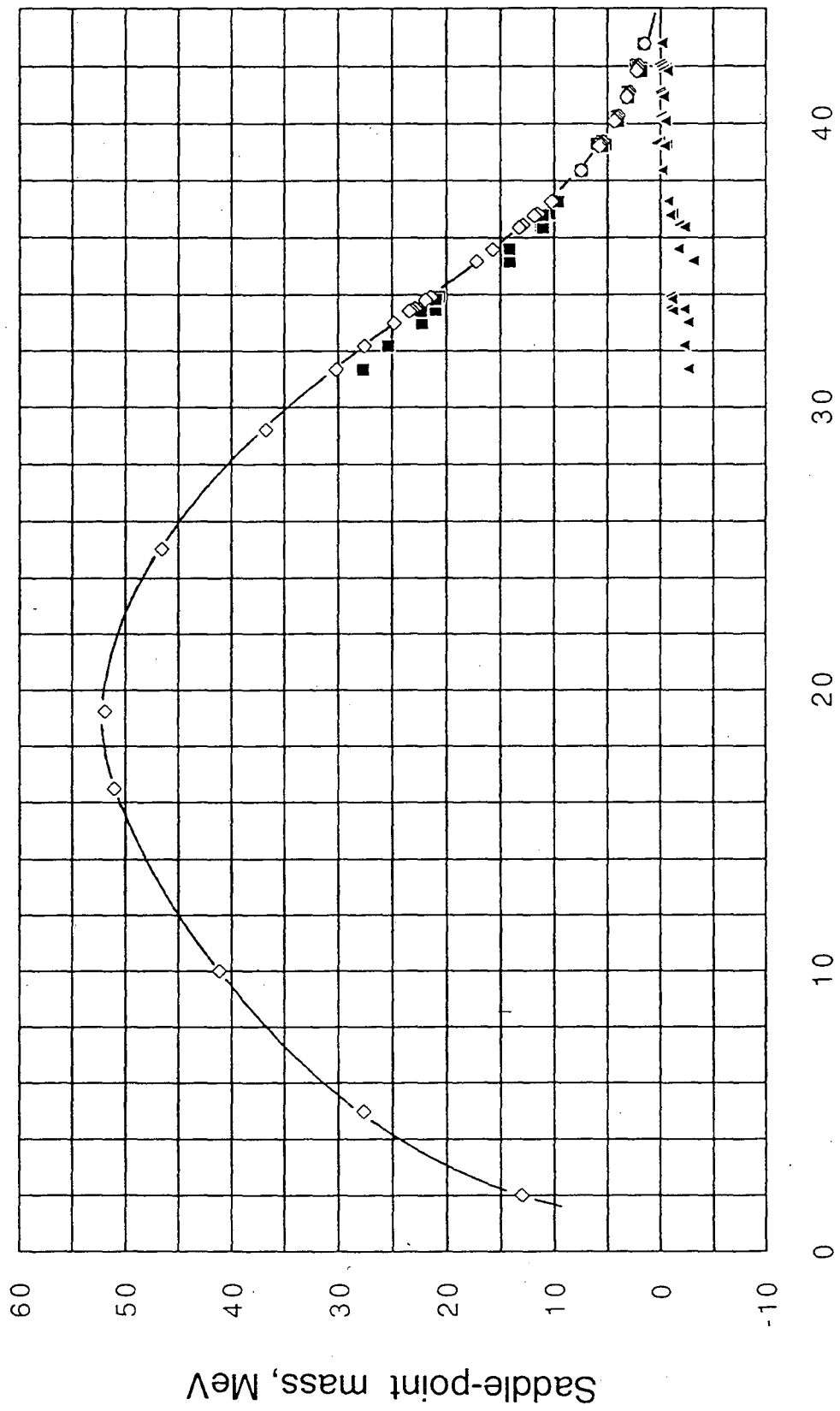


Figure 10



Fissility
Figure 11



Fissility

Figure 12

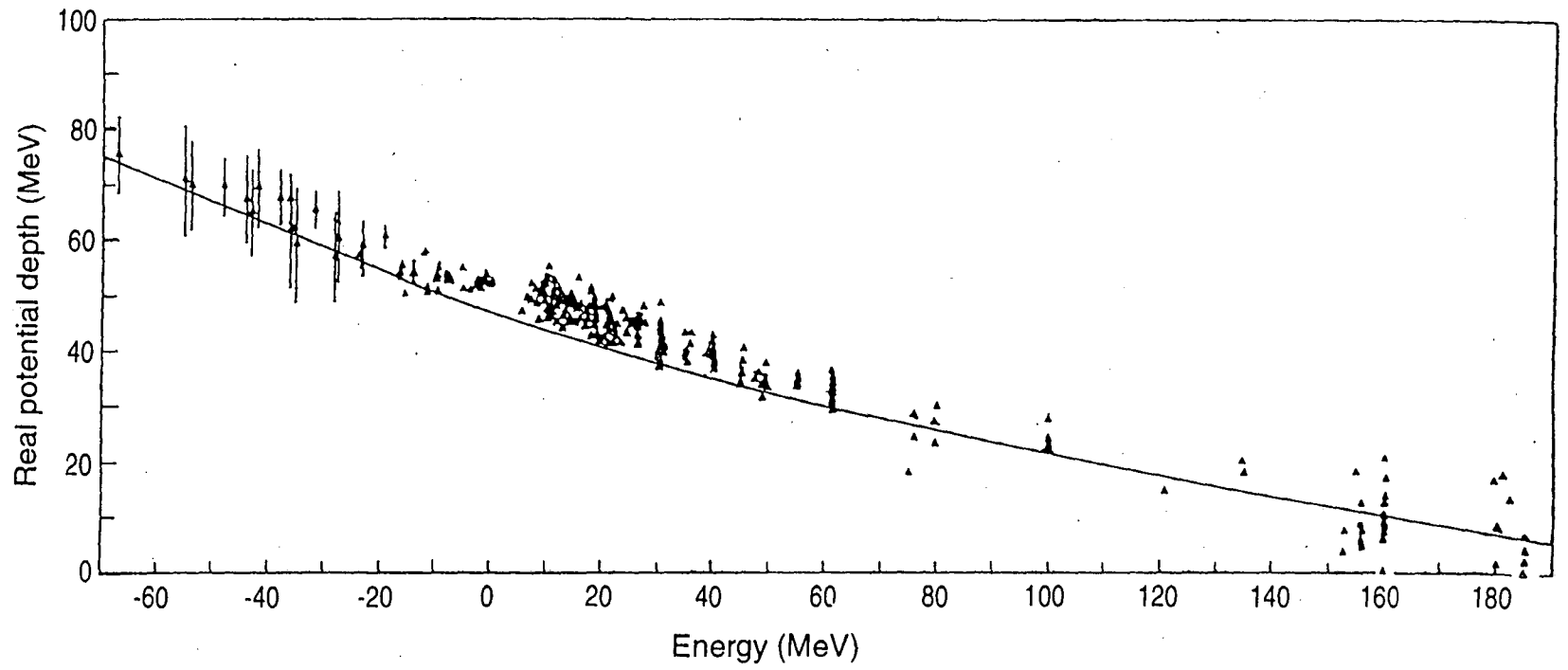


Figure 13

CHEMICAL POTENTIALS FOR TIN ISOTOPES

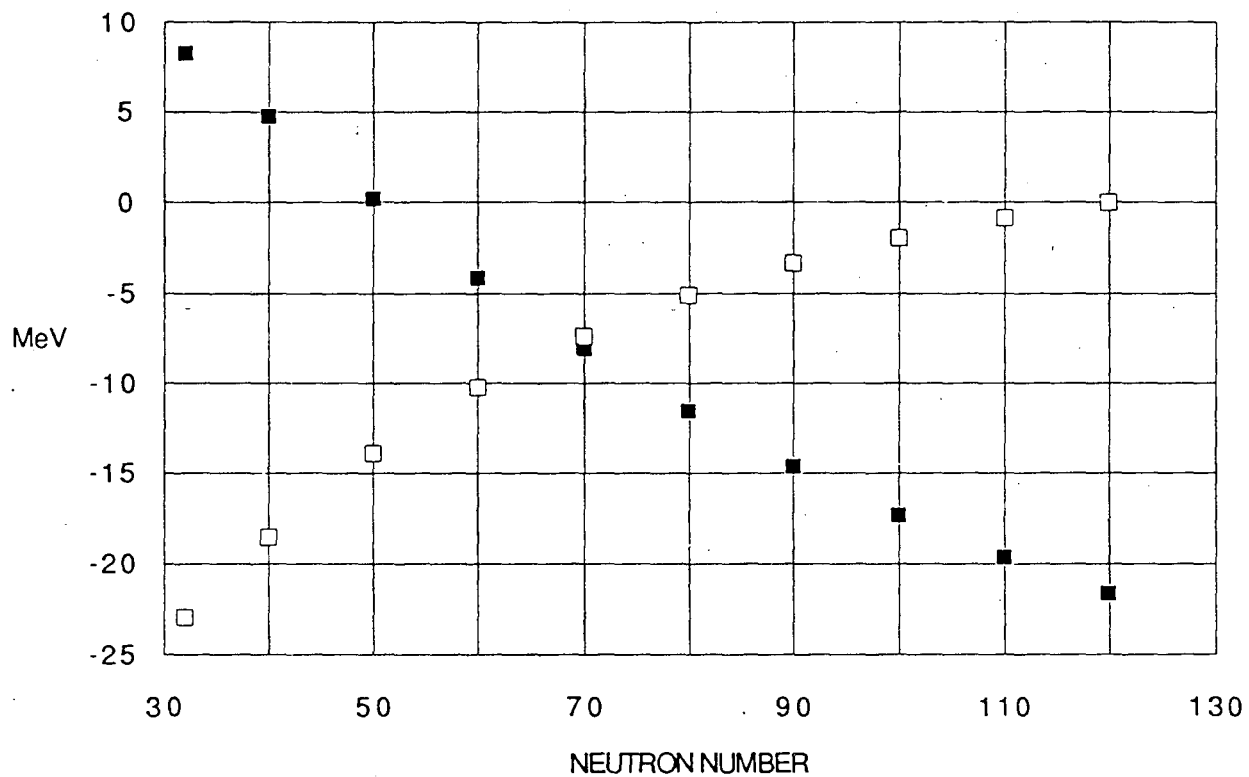


Figure 14

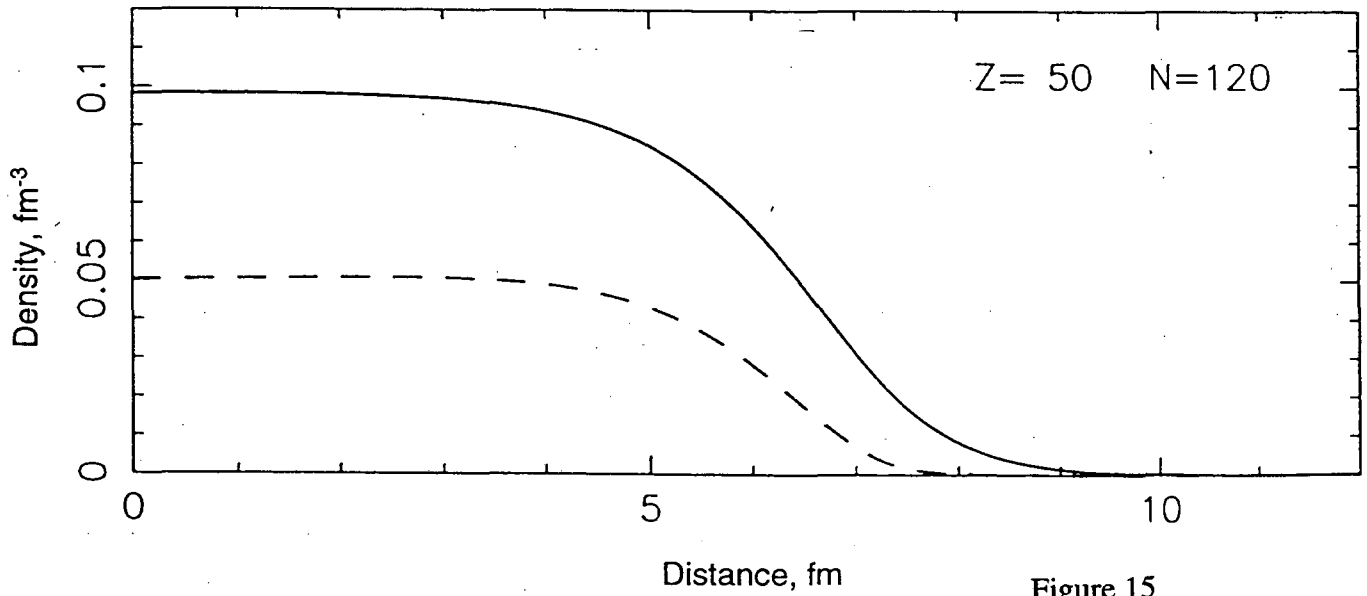
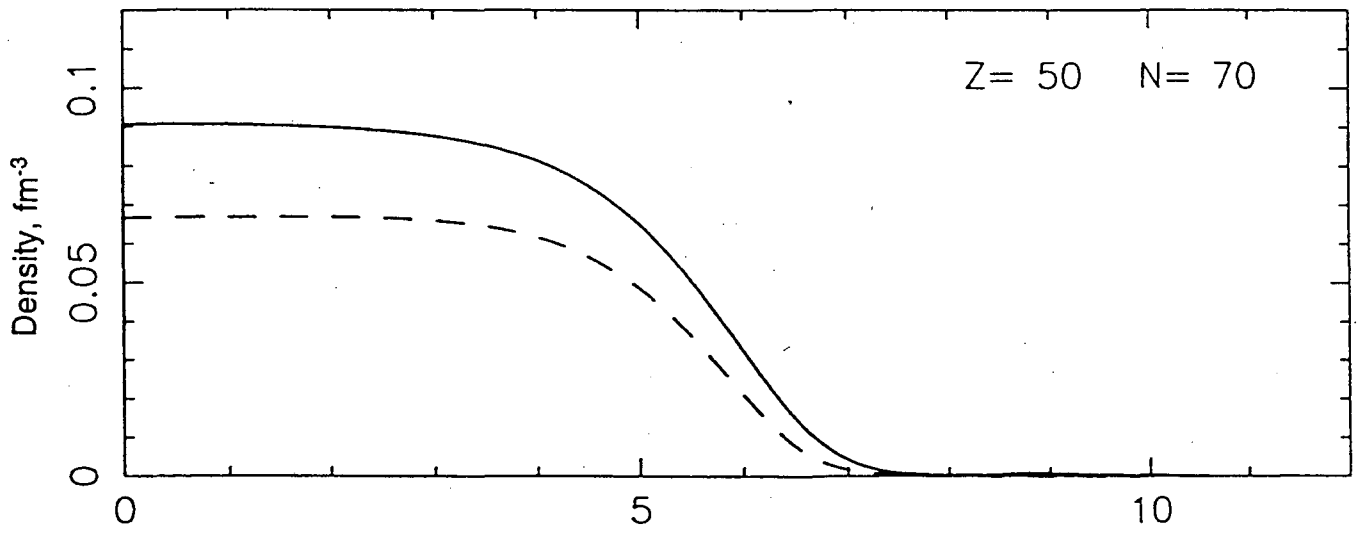
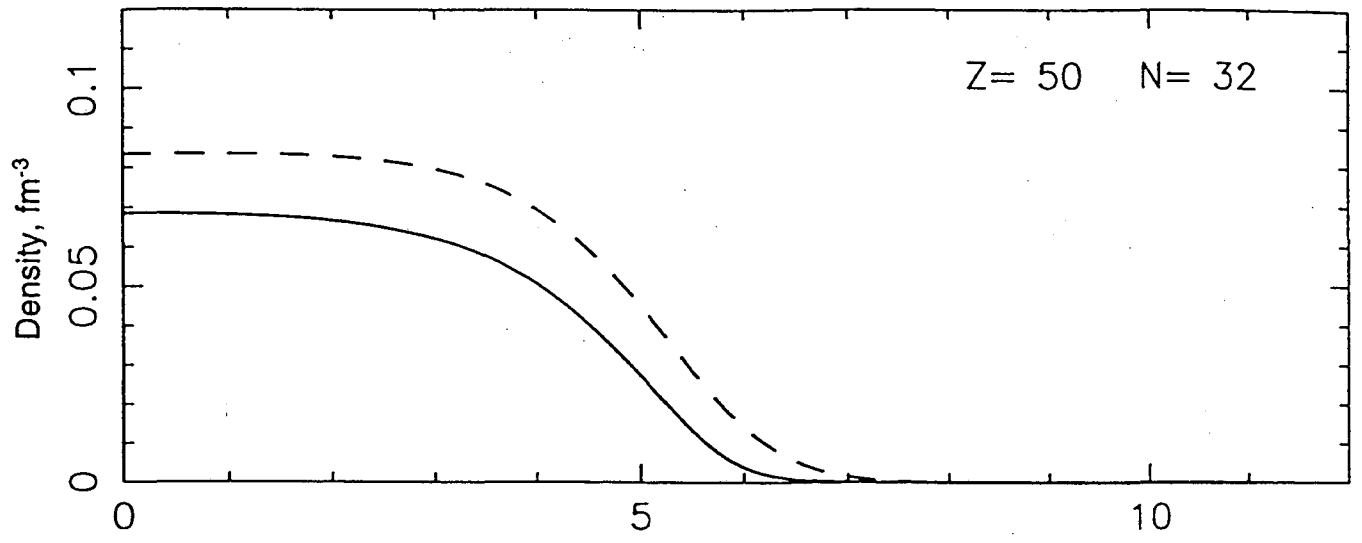


Figure 15

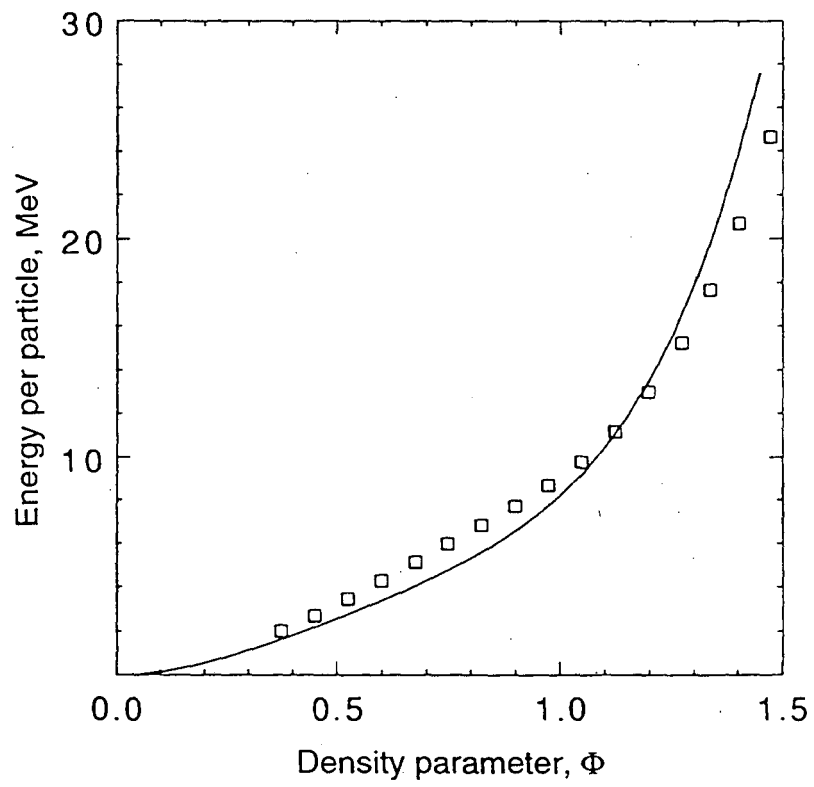


Figure 16

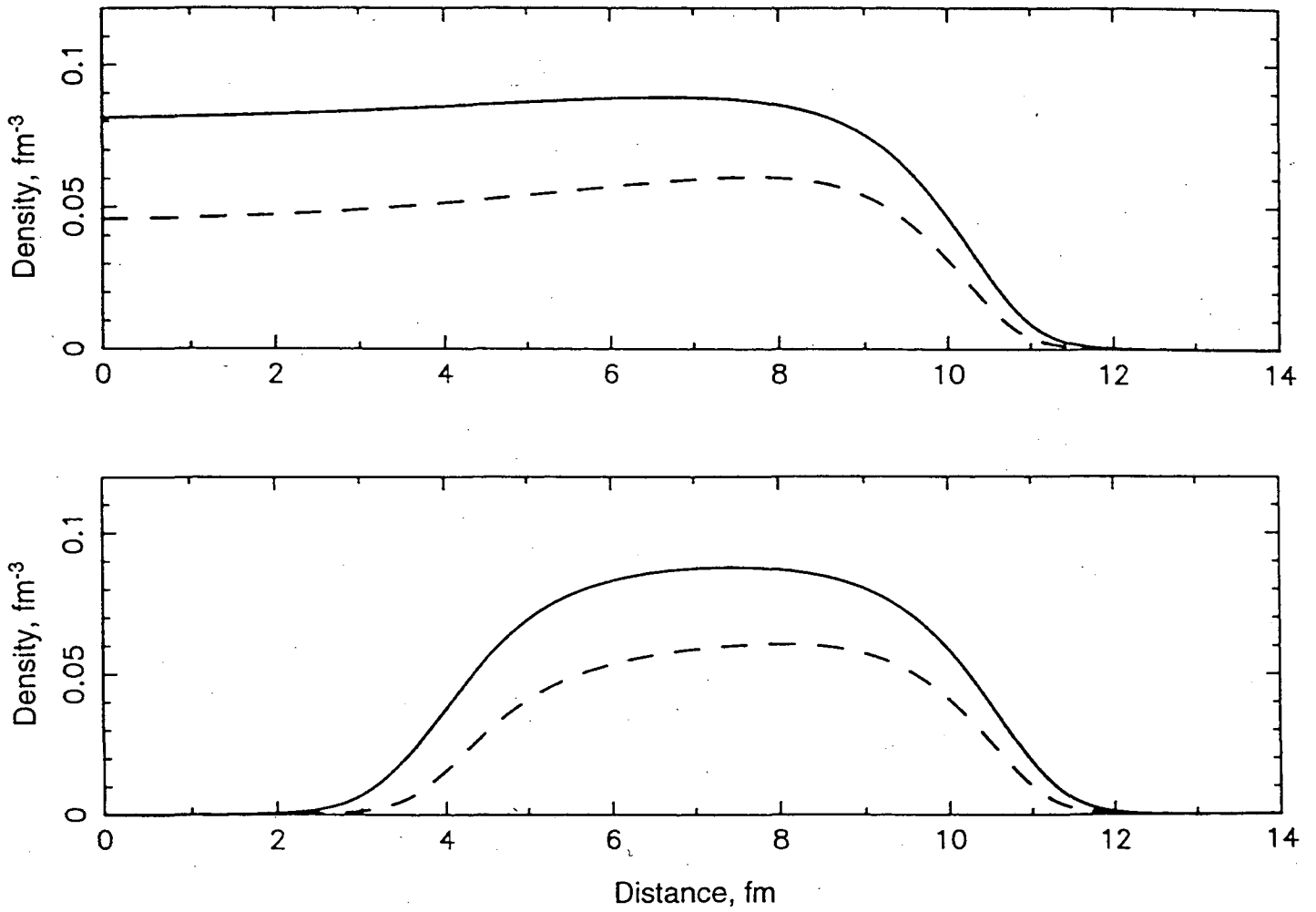


Figure 17

LAWRENCE BERKELEY LABORATORY
UNIVERSITY OF CALIFORNIA
TECHNICAL INFORMATION DEPARTMENT
BERKELEY, CALIFORNIA 94720